High Dose Neutron Irradiations of Hi-Nicalon Type S Silicon Carbide Composites, Part 1: Microstructural Evaluations

Alejandro G. Perez-Bergquist^{1,2*}, Takashi Nozawa³, Chunghao Shih¹, Keith J. Leonard¹, Lance L. Snead¹, and Yutai Katoh¹

Oak Ridge National Laboratory, Oak Ridge, Tennessee, USA
University of Tennessee, Knoxville, Tennessee, USA
Japan Atomic Energy Agency, Rokkasho, Aomori-ken, Japan

*Corresponding author address: Oak Ridge National Laboratory, PO Box 2008 MS6138, Oak Ridge TN, 37831-6138, USA. Tel.: 1-834-576-3252. E-mail: perezbergqag@ornl.gov.

Abstract

Over the past decade, significant progress has been made in the development of silicon carbide (SiC) composites, composed of near-stoichiometric SiC fibers embedded in a crystalline SiC matrix, to the point that such materials can now be considered nuclear grade. Recent neutron irradiation studies of Hi-Nicalon Type S SiC composites showed excellent radiation responses at doses of 30-40 dpa at temperatures of 300-800°C. However, more recent studies of these same fiber composites irradiated to doses of >70 dpa at similar temperatures showed a marked decrease in ultimate flexural strength, particularly at 300°C. Here, electron microscopy is used to analyze the microstructural evolution of these irradiated composites. While minimal changes are observed in Hi-Nicalon Type S SiC composites irradiated at 800°C, substantial microstructural evolutions are observed in those irradiated at 300°C, specifically in the interphase region.

1. Introduction

Continuous silicon carbide (SiC) fiber-reinforced SiC matrix composites have been considered promising structural materials for high temperature applications for decades, owing to their outstanding strength at high temperature, chemical inertness, low coefficient of thermal expansion, and added toughness and reliability derived by compositization [1-3]. For fusion energy applications, SiC composites are of particular interest due to their high radiation tolerance at elevated temperature, their low activation and decay heat properties, and their low tritium permeability [4-7].

While monolithic SiC has some applications in fusion, it fails as a structural material due to its inherent brittle nature. However, the implementation of small diameter SiC fibers into SiC composite systems has resulted in the development of SiC/SiC composites with more advantageous strength reliability and damage tolerance properties [8]. SiC/SiC composites consist of a continuous or dispersed fiber phase, a continuous matrix phase, and an interface layer or layers between the two, known as the interphase. For the fiber phase, two low-oxygen, slightly carbon-rich, near-stoichiometric SiC fibers have been developed: Hi-Nicalon Type S and Tyranno SA. Both fibers exhibit stability under high levels of neutron irradiation, and both are commercially available [9]. Pyrolytic carbon (PyC), usually deposited by chemical vapor deposition (CVD), is used as the interphase. Fracture properties of the composite may be tailored by adjusting the thickness of the PyC, and multiple layers of PyC and SiC can be used in tandem to provide resistance against

environmentally assisted cracking. SiC fibers are then woven and embedded within a polycrystalline SiC matrix. Composites formed through either chemical vapor infiltration (CVI) or nano-infiltration and transient eutectic-phase (NITE) processes have shown to exhibit good dimensional stability and strength characteristics in response to neutron irradiation [1].

Numerous studies have been performed on the neutron irradiation behavior of SiC/SiC composites [1, 2, 10-17]. In general, these nuclear-grade composites have demonstrated outstanding radiation resistance, showing minor or no degradation in proportional limit stress and ultimate strength after neutron irradiation to fluences exceeding 40 dpa at 800° C [8]. However, follow-up mechanical property examinations of Hi-Nicalon Type S SiC composites have shown substantial degradation in ultimate flexural strength at fluence levels of about 70 dpa at lower irradiation temperatures ($\sim 300^{\circ}$ C). Specifically, after irradiation to 70 dpa, strengths dropped from 335 MPa in the unirradiated state to 205 MPa at 800° C, 200 MPa at 500° C, and 95 MPa at 300° C [18]. In this work, scanning and transmission electron microscopy is used to investigate the microstructural evolution of Hi-Nicalon Type S composites after irradiation to very high fluences at temperatures of 800, 500, and 300° C.

2. Experimental Procedures

Hi-Nicalon Type-S near-stoichiometric SiC fibers (Nippon Carbon, Tokyo, Japan) were used in this study. A $0^{\circ}/90^{\circ}$ stack of two-dimensional satin weave fabrics of these fibers was coated via CVD with five thin layers of PyC (\sim 20 nm thickness) and four layers of SiC to create a multilayer interphase, followed by deposition of a polycrystalline β -phase SiC matrix using a CVI process [19].

Flexural beam test specimens machined from the CVI composite panel were neutron irradiated at the Flux Trap Facility in the High Flux Isotope Reactor (HFIR) at Oak Ridge National Laboratory to levels of \sim 71, \sim 74, and \sim 71 dpa (1 dpa \approx 1 × 10²⁵ n/m², E > 0.1 MeV) at temperatures of 800, 500, and 300°C, respectively. The irradiated specimens were cut with a diamond saw and polished using a Buehler Minimet 1000 Polisher for microstructural analysis in a Hitachi S4700 scanning electron microscope (SEM).

Transmission electron microscope (TEM) foils were fabricated from the irradiated samples via the use of an FEI Quanta Dual-beam combination focused ion beam (FIB) and SEM. Samples were fabricated so as to capture regions containing the SiC fiber, interphase, and matrix. TEM foils were analyzed in a Phillips CM 200 analytical TEM operating at 200 kV using the techniques of bright field (BF) imaging, selected area electron diffraction (SAED), high resolution TEM (HRTEM), x-ray energy dispersive spectroscopy (EDS) performed in scanning TEM (STEM) mode, high angle annular dark field (HAADF) imaging, and electron energy loss spectroscopy (EELS).

3. Results and Discussion

TEM was first performed on an unirradiated SiC/SiC composite sample to provide a comparison for the irradiated specimens. The composite system is shown in Figure 1. Part of the $\sim\!11~\mu m$ diameter fiber is shown, coated with a thin layer of PyC of $\sim\!20~nm$ in thickness. Four iterative bilayers of SiC ($\sim\!200~nm$ in thickness) and PyC ($\sim\!20~nm$ in thickness) stack upon the initial PyC layer, and CVI-deposited SiC grains compose the

matrix. SiC and PyC layers are both uniform in size and are free from the presence of voids or cracks at interfaces.

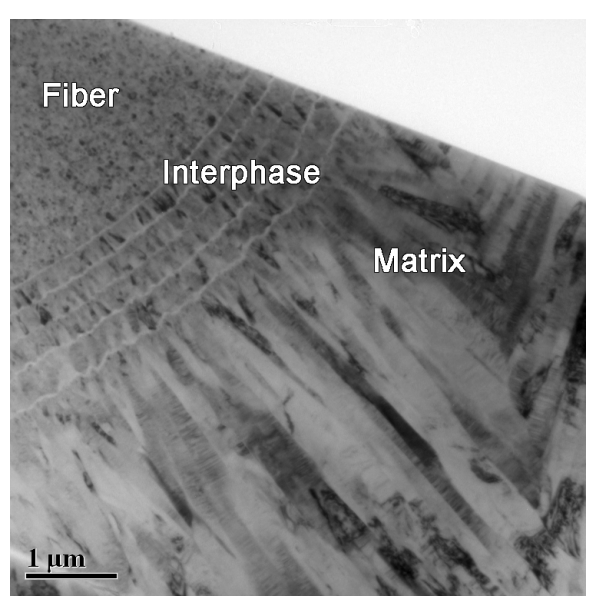


Figure 1. BF TEM image showing part of an unirradiated SiC fiber, surrounded by interphase layers and CVI-deposited SiC matrix.

Figure 2 shows SAED patterns from the unirradiated and irradiated fibers, showing no phase change in the fiber as a result of irradiation, while Figure 3 shows BF TEM images of the unirradiated fiber core and irradiated fiber cores at temperatures of 300, 500, and 800°C, respectively (Figure 3a-d). Images are all shown such that sample thickness approaches zero at the top left corner and increases towards the bottom right corner. The unirradiated fiber is composed of small SiC grains of roughly 20 to 60 nm in diameter, interspersed with irregularly-shaped secondary phase particles of anywhere from about 5 to 40 nm in size. HRTEM revealed the secondary phase regions to be solid (not void area) and lacking in crystalline order both before and after irradiation (Figure 3e), and EDS performed in STEM mode showed the secondary phases to be carbon-rich. A high angle annular dark field image of the fiber irradiated at 300°C, showing the secondary phase regions to be composed of lower-Z material than SiC, is provided in Figure 3f.

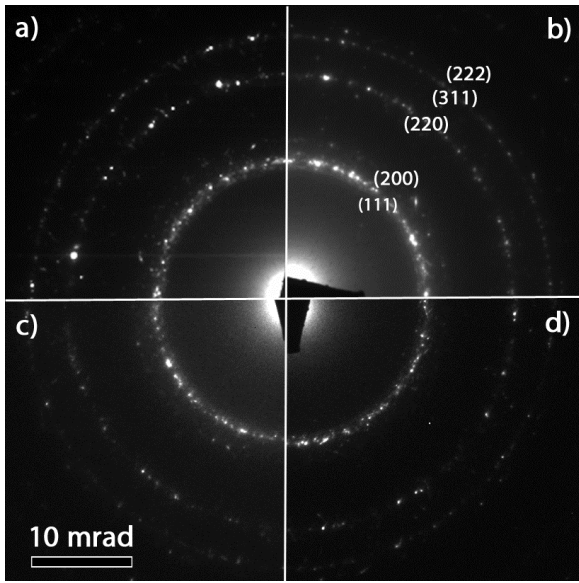


Figure 2. Diffraction patterns from the a) unirradiated fiber and from the fibers irradiated at b) 300°C, c) 500°C, and d) 800°C, showing no phase shift due to irradiation.

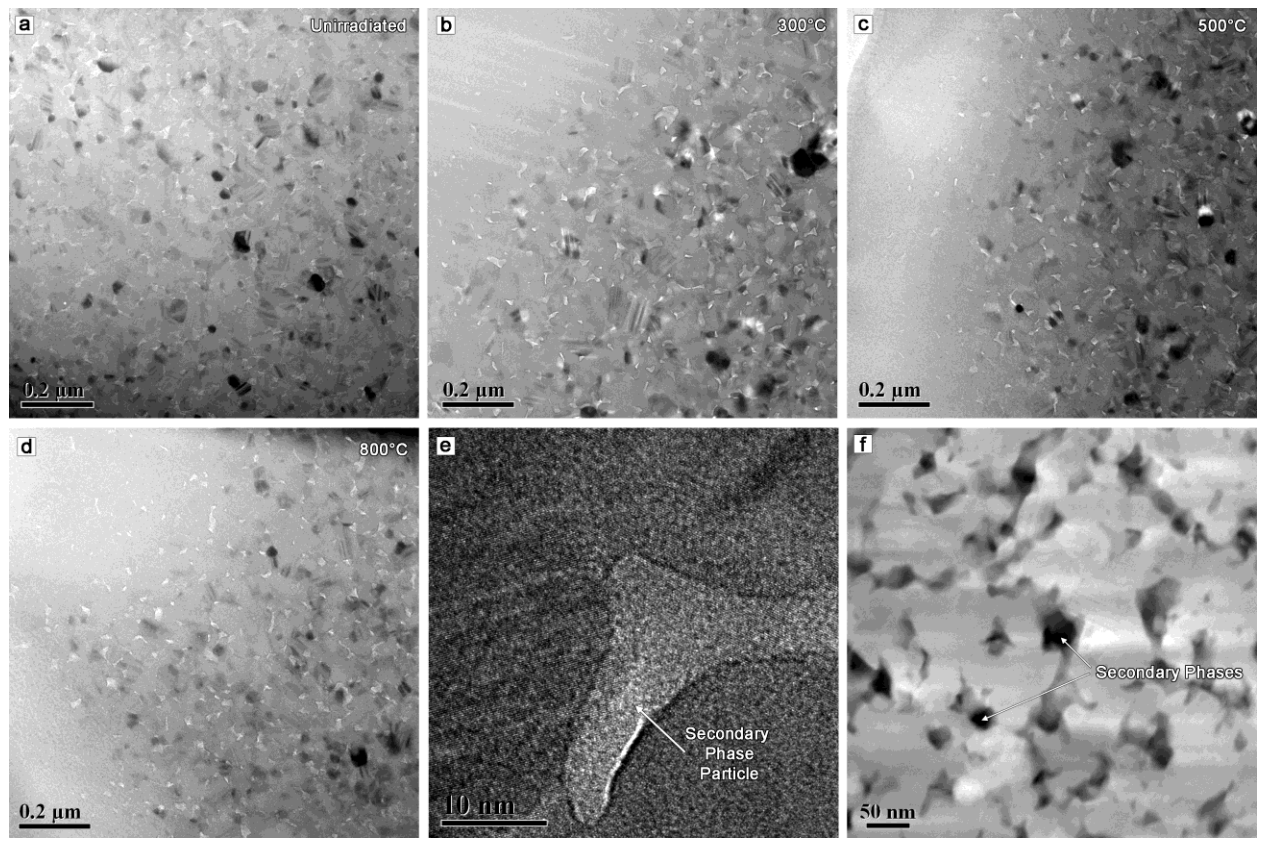


Figure 3. TEM images of the a) unirradiated fiber interior and irradiated fiber interiors at b) 300°C, c) 500°C, and d) 800°C. Film thickness approaches zero at top left corners. All fibers display reasonably similar size, distribution, and density of secondary phases. e) HRTEM image of a selected secondary phase particle after irradiation at 300°C showing a

lack of crystallinity. f) HAADF image of the fiber irradiated at 300°C, with dark regions representing secondary phases.

Size measurements of the secondary phase particles were made by drawing a line across the farthest two points of a particle, bisecting that line with a perpendicular line across the width of the particle, and averaging the two values to produce an average particle diameter. A minimum of one hundred particles was measured for each irradiated sample. Results of the measurements are shown in Table 1. The unirradiated fiber exhibited an average particle diameter of 14.8 nm, with a standard deviation of 5.9 nm. Analysis of the irradiated fibers indicated a slight increase in the secondary phase particle size with decreasing irradiation temperature, with samples irradiated at 800, 500, and 300°C displaying average particle diameters of 14.0, 15.4, and 18.5 nm, respectively. However, data set variance was substantial, as data sets had standard deviations of 5.4, 7.2, and 8.4 nm.

Given the standard deviations of the data sets, it is difficult to definitively conclude that significant changes are occurring in the size of the secondary phase particles from average particle diameters alone. However, organizing the data into histograms, as displayed in Figure 4, gives further credence to the idea that secondary phase particles are indeed growing under low-temperature irradiation. As seen in Figure 4, the most number of particles in the unirradiated fiber reside within the 10-15 nm bin, with very few particles reaching sizes of over 30 nm. The same trends hold true at 800°C. At 500°C, while the 10-15 nm bin still holds the most number of particles, the number of large particles over 30 nm in size starts to increase. At 300°C, the most populated bin shifts to the 15-20 nm range, with large numbers of particles over 30 nm in size appearing as well. Combined with the average particle sizes, the histogram data would certainly seem to indicate growth of the secondary phase, carbonaceous particles in Hi-Nicalon Type S SiC fibers under low temperature, high dose neutron irradiation.

Table 1. Size data for secondary phase particles in virgin and irradiated SiC fibers.

	Virgin	300°C	500°C	800°C
Average Particle Diameter (nm):	14.8	18.5	15.4	14.0
Median Particle Diameter (nm):	13.9	18.3	13.9	12.8
Standard Deviation (nm):	5.9	8.4	7.2	5.4

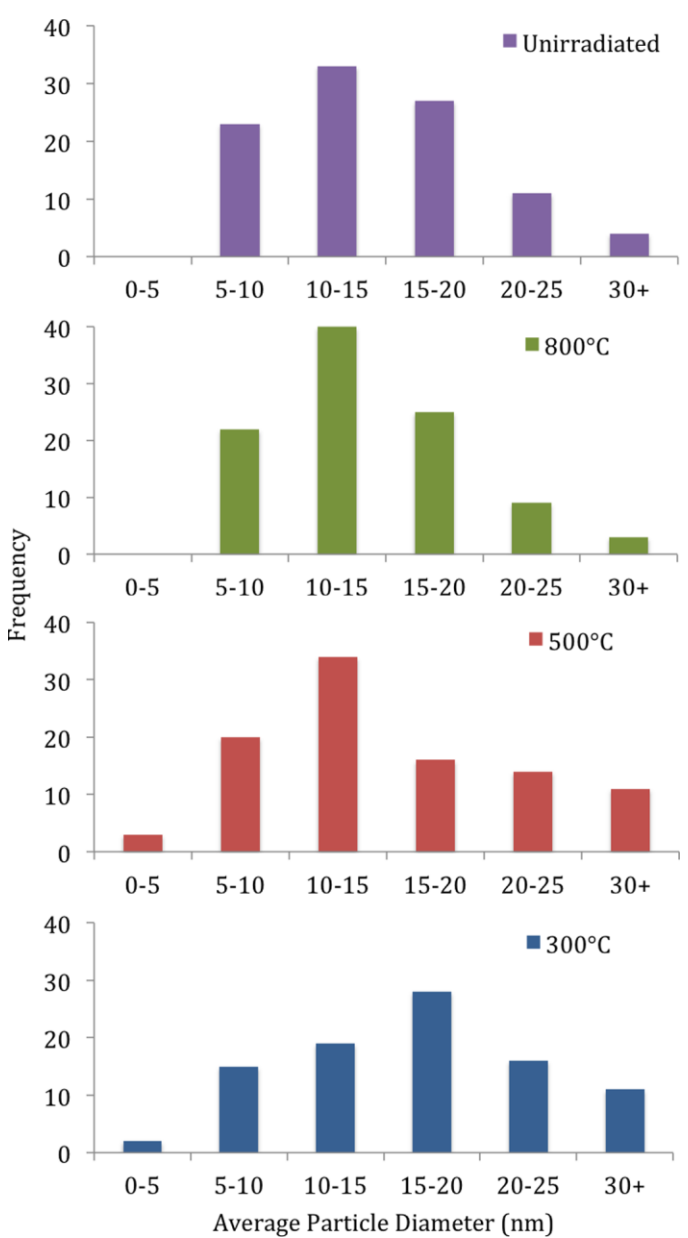


Figure 4. Histograms of the secondary phase particles in the unirradiated fiber and the fibers irradiated at 300, 500, and 800°C. Each histogram displays data for 100 particles.

While changes in TEM sample thickness made quantitative measurements difficult, qualitative perusal of the virgin and irradiated fiber regions did not seem to reveal any substantial changes in either the density or distribution of the secondary phase particles between samples. Visible irradiation damage in the fibers also seemed to be minimal. At the given irradiation levels, only black-spot damage or small dislocations loops would be expected to be found in neutron-irradiated SiC fibers [18], but even black-spot damage was found to be negligible after tilting to varying diffraction conditions in the TEM. Overall, BF TEM imagery and SAED analysis showed very limited differences between the irradiated and unirradiated SiC fibers, with the subtle change in carbonaceous particle size in the fibers irradiated at low temperature being the primary point of interest.

In the evaluation of the interphase region, however, we found a notable shift in the behavior of the irradiated specimens at different temperatures, as shown in Figure 5. Figure 5a shows an SEM micrograph of the polished surface of one of the unirradiated sets of fiber composites. The surface appeared smooth and clean, including at the interphase regions. Figure 5d, displaying the irradiated sample at 800°C, looks remarkably similar, with clean, smooth transitions between the fiber, interphase, and matrix regions. The sample irradiated at 500°C, however, exhibited some noticeable polishing damage at the fiber/interphase/matrix interfaces (Figure 5c), while the sample irradiated at 300°C showed severe cracking and degradation at the interphase (Figure 5b).

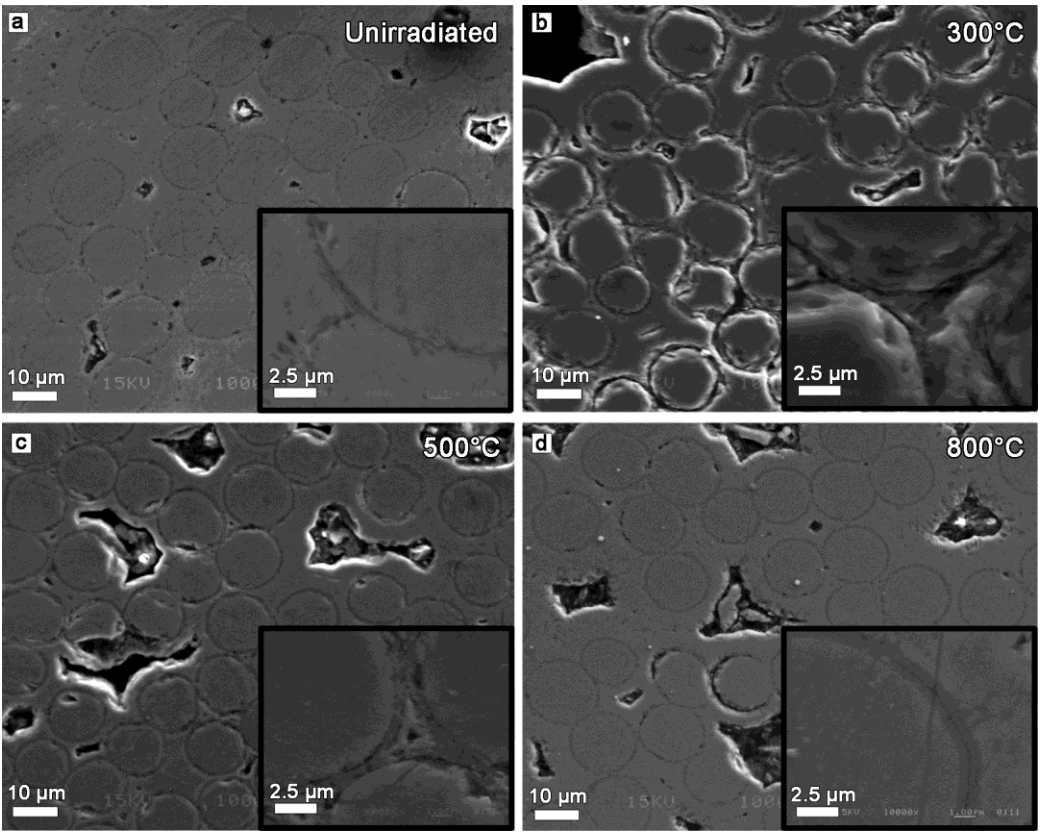


Figure 5. SEM images of a) unirradiated fibers and fibers irradiated at b) 300°C, c) 500°C, and d) 800°C. Degradation of interphase layers is more pronounced at lower temperatures.

Further investigation of the interphase regions via BF TEM showed similar results. In Figure 6a, the unirradiated interphase region is shown, while the interphase regions for the samples irradiated at 300, 500, and 800°C are shown in Figures 6b-d. Similar to the unirradiated specimen, the sample irradiated at 800°C contained four uniform SiC interphase layers separated by uniform PyC layers, with no visible deterioration of any of the deposited films. SiC layers measured about 125 nm thick, while PyC layers measured about 20 nm thick. In the sample irradiated at 500°C, only the innermost three SiC layers remained relatively uniform while the outermost layer had decomposed into discontinuous segments. SiC layers were slightly thinner on average, with a thickness of about 105 nm, while PyC layers remained relatively consistent at about 20 nm. Portions of the outermost, partially-decomposed SiC layer measured up to 140 nm thick.

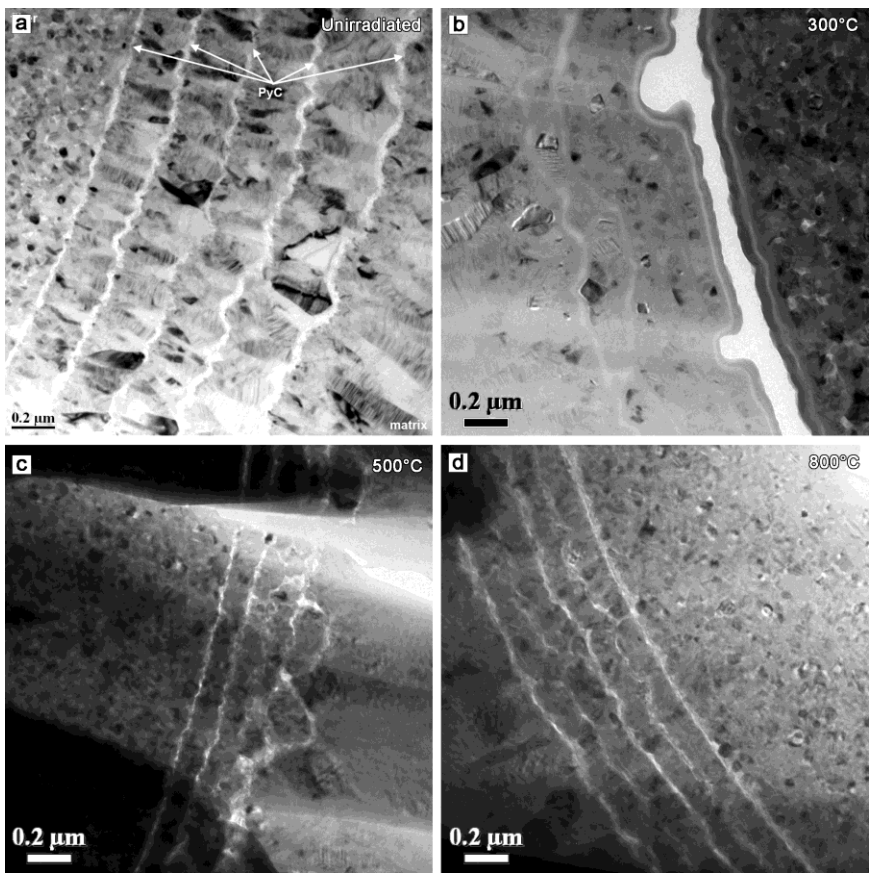


Figure 6. BF TEM images of the interphase regions from the a) unirradiated sample and irradiated samples at b) 300°C, c) 500°C, and d) 800°C. The sample irradiated at 300°C shows the greatest deterioration in the interphase, with a large gap present at the innermost PyC/SiC interface. Dark regions in c) and d) are artifacts from the FIB thinning procedure.

The most drastic differences in interphase morphology, however, were seen in the 300°C sample. As reported earlier, initial SiC layer thicknesses were measured at about 200 nm. In the sample irradiated at 800°C, average SiC layer thickness was measured at 125 nm, while the layer thickness was measured at 105 nm in the sample irradiated at 500°C. A further drop in thickness was observed in the sample irradiated at 300°C, which exhibited continuous, crystalline layers with a thickness of just 80 nm. While there is statistical uncertainty involved in the measurement of these layers due to limited sampling within the TEM, the data nonetheless indicates a significant drop in SiC layer thickness after irradiation, with an inverse correlation between SiC layer thickness and temperature.

In addition, the layers in the 300°C sample were substantially more irregular than in the other specimens, and as in the 500°C sample, the outermost layer was observed to have decomposed into thick, discontinuous segments, some of which measured up to 150~nm thick. Perhaps the most stark difference visible in the 300°C sample was in the morphology of the layers that had previously consisted solely of PyC. For one, these layers increased in thickness, up to an average of about 40~nm with select regions approaching 70~nm. In addition, HRTEM of the SiC/formerly-PyC layer interfaces did not show the characteristic,

turbostratic graphite texture of PyC [20], but instead showed fully amorphous contrast, indicating that the layers may have transformed from PyC to an amorphous mixture of both carbon and SiC, as evidenced by the decrease in the polycrystalline SiC layer thicknesses. HRTEM images of the SiC/PyC layer interface in the unirradiated condition and the SiC/formerly-PyC layer interface after irradiation at 300°C are shown in Figure 7.

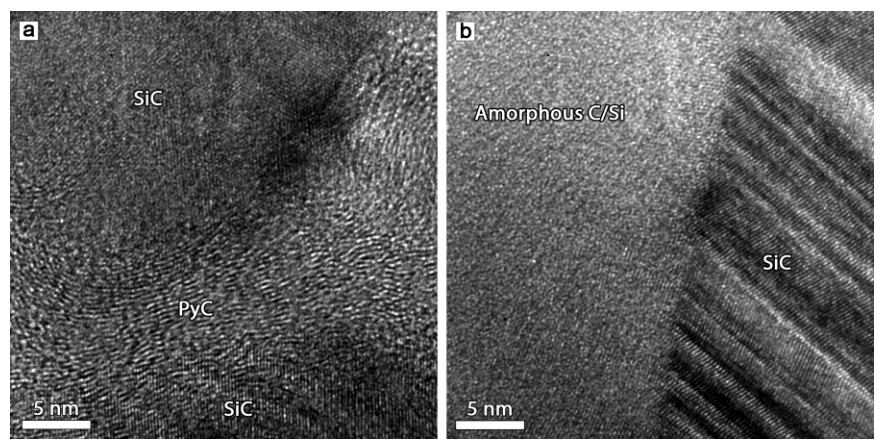


Figure 7. HRTEM images of a) SiC and PyC layers in the unirradiated specimen and b) the SiC/formerly-PyC layer interface in the sample irradiated at 300°C. Notice that the turbostratic texture of the PyC becomes fully amorphous after high dose irradiation at this temperature.

In addition, a large gap of about 100 nm in thickness developed between the fiber and innermost SiC layer, seemingly bifurcating the innermost amorphous carbon layer, and large, void-like openings (visible in Figure 5b, likely artifacts of sample preparation process) punctuated the gap. A region of slightly darker contrast existed at the gap interface, which EDS revealed to be due to a Ga-rich layer at the outer edge of the amorphous carbon (also due to sample fabrication). Given that the gap was found to be present before final sample thinning, as well as the fact that such a gap was not found in the unirradiated sample or the samples irradiated at 500 and 800°C, we do not believe the gap to be an artifact of the sample preparation process, although its magnitude may have been exacerbated by said process.

Additional TEM analysis of the matrix regions revealed dense, pore-free material with limited irradiation damage. In addition, no cracking or changes in morphology were observed in the matrix regions.

Though the observed changes in the fiber interphase are significant, the deterioration of the interphase layers is not suspected to be responsible for the large observed drop in flexural strength in the 300°C sample [18]. Fiber matrix composites are designed to mitigate brittle fracture; cracks propagating through composites should dissipate at fiber/matrix interfaces. Though deterioration of the interphase could result in reduced proportional limit stresses, such behavior should not result in lowered ultimate strengths of the composite as a whole [21]. Only changes in morphology or phase of the fiber itself should result in decreases in ultimate strength of the composite.

With that said, we must conclude that the minor changes in secondary phase particle size are responsible for the observed changes in flexural strength of the fibers. But

that begs the questions, what is responsible for the growth of the particles? Diffraction patterns (Figure 2) did not indicate any change in fiber phase. However, since the fibers are primarily composed of SiC, subtle phase changes of the carbonaceous particles within the fibers are not readily visible through the SAED patterns. Even though HRTEM indicated that these particles were amorphous, EELS was performed on the fibers to see if any subtle phase shift was occurring in these secondary phase regions.

Figure 8 shows the results of the EELS tests, with spectra shown at an energy loss region that is relevant to carbon. All fibers showed a strong sigma* (σ *) peak at about 295 eV, but no pi* (π *) peak was observed at about 285 eV. The lack of a π * peak would seem to indicate that the carbon in the secondary phase particles is more diamond-like than graphitic or purely amorphous [22], but then again, the lack of this peak may be due to curve smoothening due to the overwhelming presence of SiC, and not just carbon, in the fibers. More importantly however, there is a clear peak in the unirradiated fiber at about 308 eV. This peak is less pronounced at 800 and 500°C and is nearly gone at 300°C. While the precise nature of this phase shift is unknown, the fact that the shift is most pronounced in the 300°C sample seems to indicate that this shift may be correlated to the growth of the carbonaceous particles and, correspondingly, may be responsible for the observed embrittlement in the SiC fibers at this temperature.

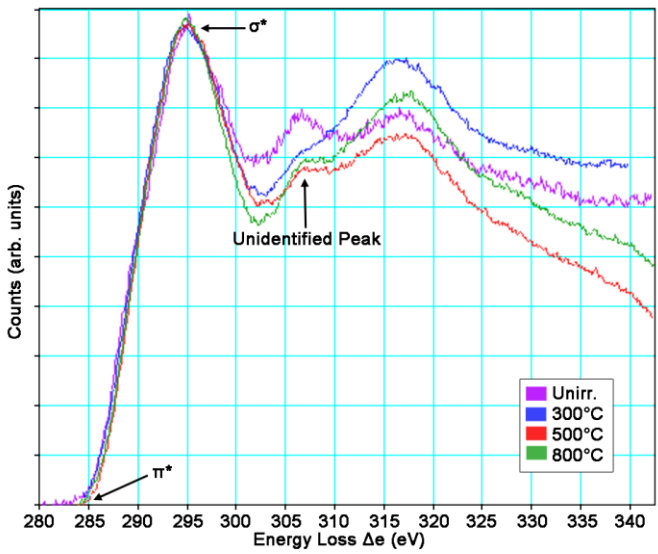


Figure 8. EELS spectra of the unirradiated fiber and the fibers irradiated at 300, 500, and 800°C.

4. Conclusions

A Hi-Nicalon Type S SiC fiber, CVI SiC matrix composite was irradiated to levels of >70 dpa at temperatures of 300, 500, and 800°C, and decreases in ultimate flexural strength were observed in the lower temperature samples, most notably the sample tested at 300°C. Microstructural evaluations showed a small but significant change in the size of carbonaceous particles in the fibers that had been irradiated at lower temperatures. Cracking was also observed at the innermost fiber/PyC interfaces, with extensive damage to the entire interphase visible at 300°C. While electron diffraction did not reveal any change in phase of the SiC fibers, EELS analysis indicated a slight phase shift in the

carbonaceous secondary particles present within said fibers, with the greatest shift detected in the fibers irradiated at 300°C. While further work is needed to fully explain both the nature and reason for the observed changes, growth and phase shift of carbonaceous particles in the fibers are suspected to play a critical role in the embritlement of the fibers following irradiation.

Acknowledgements

This research was sponsored by the Office of Fusion Energy Sciences, U.S. Department of Energy under contract DE-AC05-000R22725 with UT-Battelle, LLC. The TEM characterization utilized ORNL's Shared Research Equipment (ShaRE) User Facility, which is sponsored by the Scientific User Facilities Division, Office of Basic Energy Sciences, U.S. Department of Energy.

References

- [1] Y. Katoh, L.L. Snead, C.H. Henager Jr., A. Hasegawa, A. Kohyama, B. Riccardi, H.Hegeman, *J. Nucl. Mater.* **367–370** (2007) 659-671.
- [2] L.L. Snead, R.H. Jones, A. Kohyama, P. Fenici, J. Nucl. Mater. 233-237 (1996) 26-36.
- [3] A. Kohyama, M. Seki, K. Abe, T. Muroga, H. Matsui, S. Jitsukawa, S. Matsuda, *J. Nucl. Mater.* **283–287** (2000) 20-27.
- [4] R.J. Price, J. Nucl. Mater. 33 (1969) 17-22.
- [5] R.J. Price, Nucl. Technol. 35 (1977) 320-336.
- [6] T. Noda, M. Fujita, H. Araki, A. Kohyama, Fusion Eng. Des. 61-62 (2002) 711-716.
- [7] R.A. Causey, W.R. Wampler, J. Nucl. Mater. 220-222 (1995) 823-826.
- [8] L.L. Snead, T. Nozawa, M. Ferraris, Y. Katoh, R. Shinavski, M. Sawan, *J. Nucl. Mater.* **417** (2011) 330-339.
- [9] P. Fenici, A.J. Frias Rebelo, R.H. Jones, A. Kohyama, L.L. Snead, *J. Nucl. Mater.* **258-263** (1998) 215-225.
- [10] T. Nozawa, T. Hinoki, L.L. Snead, Y. Katoh, A. Kohyama, *J. Nucl. Mater.* **329-333** (2004) 544–548.
- [11] Y. Katoh, A. Kohyama, T. Nozawa, M. Sato, *J. Nucl. Mater.* **329–333** (2004) 587–591.
- [12] Y. Katoh, T. Nozawa, L.L. Snead, T. Hinoki, J. Nucl. Mater. **367–370** (2007) 774–779.
- [13] Y. Katoh, T. Nozawa, L.L. Snead, T. Hinoki, A. Kohyama, *Fusion Eng. Des.* **81** (2006) 937–944.
- [14] Y. Katoh, T. Nozawa, L.L. Snead, K. Ozawa, H. Tanigawa, *J. Nucl. Mater.* **417** (2011) 400–405.
- [15] T. Nozawa, Y. Choi, T. Hinoki, H. Kishimoto, A. Kohyama, H. Tanigawa, *IOP Conf. Series: Mater. Sci. Eng.* **18** (2011) 162011.
- [16] L.L. Snead, Y. Katoh, A. Kohyama, J.L. Bailey, N.L. Vaughn, R.A. Lowden, *J. Nucl. Mater.* **283–287** (2000) 551–555.
- [17] Y. Katoh, K. Ozawa, T. Hinoki, Y. Choi, L.L. Snead, A. Hasegawa, *J. Nucl. Mater.* **417** (2011) 416-420.
- [18] Y. Katoh, T. Nozawa, A.M. Williams, T. Cheng, P. Dou, L.L. Snead, Properties of Hi-Nicalon Type-S CVI SiC Composites Irradiated to 70 dpa at Elevated Temperatures. ORNL/TM-2012/459, September 30, 2012.

- [19] G. Newsome, L.L. Snead, T. Hinoki, Y. Katoh, D. Peters, J. Nucl. Mater. 371 (2007) 76-89.
- [20] J.Y. Yan, C.W. Chen, P.C. Fang, K.M. Yin, F.R. Chen, Y. Katoh, A. Kohyama, J.J. Kai, *J. Nucl. Mater.* **329–333** (2004) 513–517.
- [21] A.G. Evans and F.W. Zok, J. Mater. Sci. 29 (1994) 3857-3896.
- [22] J. Robertson, Semicond. Sci. Technol. 18 (2003) S12-S19.